



HAL
open science

Constraints for the Martian Crustal Structure From Rayleigh Waves Ellipticity of Large Seismic Events

Sebastián. Carrasco, Brigitte Knapmeyer-Endrun, Ludovic Margerin, Zongbo Xu, Rakshit Joshi, Martin Schimmel, Eleonore Stutzmann, Constantinos Charalambous, Philippe Lognonné, W. Bruce Banerdt

► **To cite this version:**

Sebastián. Carrasco, Brigitte Knapmeyer-Endrun, Ludovic Margerin, Zongbo Xu, Rakshit Joshi, et al.. Constraints for the Martian Crustal Structure From Rayleigh Waves Ellipticity of Large Seismic Events. *Geophysical Research Letters*, 2023, 50, 10.1029/2023GL104816 . insu-04199338

HAL Id: insu-04199338

<https://insu.hal.science/insu-04199338>

Submitted on 7 Sep 2023

HAL is a multi-disciplinary open access archive for the deposit and dissemination of scientific research documents, whether they are published or not. The documents may come from teaching and research institutions in France or abroad, or from public or private research centers.

L'archive ouverte pluridisciplinaire **HAL**, est destinée au dépôt et à la diffusion de documents scientifiques de niveau recherche, publiés ou non, émanant des établissements d'enseignement et de recherche français ou étrangers, des laboratoires publics ou privés.



Distributed under a Creative Commons Attribution - NonCommercial - NoDerivatives 4.0
International License

Geophysical Research Letters[®]











RESEARCH LETTER

10.1029/2023GL104816

Special Section:

The Large Marsquake of Sol 1222

Constraints for the Martian Crustal Structure From Rayleigh Waves Ellipticity of Large Seismic Events

Sebastián Carrasco¹ , Brigitte Knapmeyer-Endrun², Ludovic Margerin³, Zongbo Xu⁴ , Rakshit Joshi⁵ , Martin Schimmel⁶ , Eleonore Stutzmann⁴ , Constantinos Charalambous⁷ , Philippe Lognonné⁴ , and W. Bruce Banerdt⁸ 

Key Points:

- Rayleigh waves ellipticity was measured between periods 15–35 s at the InSight landing site using large seismic events, including S1222a
- A 4-layer crust, including a shallow low-velocity layer, is required to explain the ellipticity, receiver functions and P-wave lag times
- Low crustal velocities are derived for the InSight site, which may be due to high porosity or heavy alteration at local scale

Supporting Information:

Supporting Information may be found in the online version of this article.

Correspondence to:

S. Carrasco,
acarrasc@uni-koeln.de

Citation:

Carrasco, S., Knapmeyer-Endrun, B., Margerin, L., Xu, Z., Joshi, R., Schimmel, M., et al. (2023). Constraints for the Martian crustal structure from Rayleigh waves ellipticity of large seismic events. *Geophysical Research Letters*, 50, e2023GL104816. <https://doi.org/10.1029/2023GL104816>

Received 19 JUN 2023
Accepted 13 AUG 2023

Author Contributions:

Conceptualization: Sebastián Carrasco, Brigitte Knapmeyer-Endrun, Ludovic Margerin, Zongbo Xu, Rakshit Joshi, Martin Schimmel, Eleonore Stutzmann
Data curation: Sebastián Carrasco, Constantinos Charalambous
Formal analysis: Sebastián Carrasco, Constantinos Charalambous

© 2023 The Authors.

This is an open access article under the terms of the [Creative Commons Attribution-NonCommercial License](https://creativecommons.org/licenses/by-nc/4.0/), which permits use, distribution and reproduction in any medium, provided the original work is properly cited and is not used for commercial purposes.

¹Bensberg Observatory, University of Cologne, Bergisch Gladbach, Germany, ²Microgravity User Support Center, German Aerospace Center (DLR), Cologne, Germany, ³Institut de Recherche en Astrophysique et Planétologie, Université Toulouse III Paul Sabatier, CNRS, CNES, Toulouse, France, ⁴Université Paris Cité, Institut de physique du globe de Paris, CNRS, Paris, France, ⁵Max Planck Institute for Solar System Research, Göttingen, Germany, ⁶Geosciences Barcelona, CSIC, Barcelona, Spain, ⁷Department of Electrical and Electronic Engineering, Imperial College London, London, UK, ⁸Jet Propulsion Laboratory, California Institute of Technology, Pasadena, CA, USA

Abstract For the first time, we measured the ellipticity of direct Rayleigh waves at intermediate periods (15–35 s) on Mars using the recordings of three large seismic Martian events, including S1222a, the largest event recorded by the InSight mission. These measurements, together with P-to-s receiver functions and P-wave reflection times, were utilized for performing a joint inversion of the local crustal structure at the InSight landing site. Our inversion results are compatible with previously reported intra-crustal discontinuities around 10 and 20 km depths, whereas the preferred models show a strong discontinuity at ~37 km, which is interpreted as the crust-mantle interface. Additionally, we support the presence of a shallow low-velocity layer of 2–3 km thickness. Compared to nearby regions, lower seismic wave velocities are derived for the crust, suggesting a higher porosity or alteration of the whole local crust.

Plain Language Summary As never before on Mars, we measured the characteristics of seismic waves traveling along the Martian surface that carry information about the crustal structure at the InSight site. We combined these measurements with two other local-scale independent observations to derive a consolidated model for the crust underneath the InSight lander. Our results suggest a Martian crust with 4 layers and, particularly, one thin layer of about 2 km thickness close to the surface. The crust-mantle discontinuity was found at ~37 km depth, where the sharpest change in seismic wave velocity is observed. Overall, the seismic wave velocities of the local Martian crust at the InSight site are lower than those derived in other regions on Mars, which suggests a higher porosity or local alteration.

1. Introduction

The structure and properties of the Martian crust are important for understanding the evolution of Mars and rocky planets. In this context, the InSight mission (Banerdt et al., 2020), which landed on Elysium Planitia in November 2018, aims to study the interior of Mars by means of one seismological station placed on the Martian surface (Lognonné et al., 2019).

After more than 3 years of data collection, the Martian crust has been studied by a thorough analysis of the InSight seismological data. Locally at the InSight landing site, early analysis of P-to-s receiver functions (RFs) allowed to derive a shallow layer with low seismic velocities in the first 8–11 km of the Martian crust (Lognonné et al., 2020). Further investigation including more marsquakes suggests a layered local Martian crust with two discontinuities at 8 ± 2 km and 20 ± 5 km, and a bimodal estimation of the crust thickness of either 20 ± 5 or 39 ± 8 km (Knapmeyer-Endrun et al., 2021). Subsequently, the analysis of further seismic events and the identification of other secondary phases (PPs, Sp and three new crustal multiples) favor a 3-layer crustal model (Joshi et al., 2023; Kim et al., 2021), for which the crust-mantle boundary would be located at ~40 km depth. The shallow discontinuity around 8 km depth has been confirmed by the detection of SsPp phases (J. Li, Beghein, Davis, et al., 2022) and SH-wave reflections (J. Li, Beghein, Wookey, et al., 2022). Recently, Shi et al. (2023) proposed a shallow discontinuity at around 2 km depth, based on the analysis of high-frequency RFs. Further properties and characteristics of the Martian crust at regional scales (e.g., Kim, Banerdt, et al., 2022; Beghein et al., 2022; Kim, Stähler, et al., 2022; J. Li, Beghein, Lognonné, et al., 2022), as well as at global scale and away from the lander

Funding acquisition: W. Bruce Banerdt

Investigation: Sebastián Carrasco, Constantinos Charalambous

Methodology: Sebastián Carrasco, Brigitte Knapmeyer-Endrun, Ludovic Margerin, Zongbo Xu, Rakshit Joshi, Martin Schimmel, Eleonore Stutzmann

Project Administration: Philippe Lognonné, W. Bruce Banerdt

Resources: Sebastián Carrasco, Brigitte Knapmeyer-Endrun

Software: Sebastián Carrasco, Rakshit Joshi

Supervision: Brigitte Knapmeyer-Endrun

Validation: Sebastián Carrasco

Visualization: Sebastián Carrasco

Writing – original draft: Sebastián Carrasco, Brigitte Knapmeyer-Endrun

Writing – review & editing: Sebastián Carrasco, Brigitte Knapmeyer-Endrun,

Ludovic Margerin, Zongbo Xu, Rakshit Joshi, Martin Schimmel, Eleonore

Stutzmann, Philippe Lognonné

(e.g., J. Li, Beghein, McLennan, et al., 2022; Wiczcerek et al., 2022; Durán et al., 2022), have been derived from the analysis of the InSight seismic data using different approaches. Table S1 in Supporting Information S1 details some representative models for the Martian crust.

Besides RFs, the analysis and inversion of the ellipticity of direct Rayleigh waves is a single-station technique that, when measured at intermediate and long periods (>10 s), allows investigating the local underground structure down to crustal depths (Tanimoto & Rivera, 2008; Yano et al., 2009). The ellipticity, understood as the ratio between the radial (R) and the vertical (Z) ground-motion of the Rayleigh wave (Figure 1a), has been shown to be invariant to the seismic source, the wave propagation path or the epicentral distance and rather depend on the local structure directly beneath the receiver (e.g., Ferreira & Woodhouse, 2007). Even though this methodology was proposed in the 1970s, it has gained popularity only in recent years and with successful applications on Earth (e.g., Lin et al., 2012; G. Li et al., 2016; Berbellini et al., 2017), but it has not been applied on Mars so far due to the lack of observation of direct Rayleigh waves. Hence, the ellipticity analysis of direct Rayleigh waves is still a pending task that could provide further constraints on the structure of the Martian crust at the InSight landing site, as proposed by Panning et al. (2017).

On 4 May 2022, the InSight lander recorded the S1222a event, which had a moment magnitude estimated as M_w 4.7 and thus corresponds to the largest seismic event ever recorded on Mars (Kawamura et al., 2022). This event exhibits clear surface waves (both Love and Rayleigh) that can be used for studying lithospheric properties along the source-receiver path (e.g., Beghein et al., 2022; J. Li, Beghein, Lognonné, et al., 2022; Kim, Stähler, et al., 2022; Xu et al., 2023), but is also a unique opportunity to investigate the local crustal structure through ellipticity analysis of Rayleigh waves. Similarly, the events S1000a and S1094b are two other good-quality seismic events, which are related to the impact of meteorites on the Martian surface, 126° and 58° away from the InSight lander, and had magnitudes estimated as M_w 4.1 and 4.0, respectively (Posiolova et al., 2022). For these two events, Rayleigh waves have also been observed (Kim, Banerdt, et al., 2022). These three large events, whose source locations are shown in Figure 1b, are thus excellent candidates to perform a Rayleigh wave ellipticity (also referred to as ϵ) analysis.

The analysis of ϵ data can be used as an independent observation to characterize the Martian crust at the InSight landing site. The inversion of RFs is affected by the non-uniqueness phenomenon and, although these data are highly sensitive to discontinuities, the addition of ϵ data can provide constraints on long-wavelength velocity features (Chong et al., 2016). As both data sets map the local structure at similar local scales, a joint inversion of ϵ and P-to-s RFs can be performed. Similarly, the autocorrelation times (hereafter T_a) obtained from the analysis of seismic ambient noise, such as those by Schimmel et al. (2021), are sensitive to the local crustal structure and therefore can be used as an independent data set to constrain the inversion. In fact, the predicted T_a for the crustal models in Table S1 in Supporting Information S1 differs from the measurements (Table S3 in Supporting Information S1) whereas, as shown in Figure 2a, the corresponding predicted ellipticity curves fail to match the measured ϵ . These mismatches further encourage a joint inversion of the three data sets.

In this work, we analyze the ellipticity and phase shift of the Rayleigh waves related to the large seismic events S1000a, S1094b and especially S1222a, to obtain further constraints on the structure of the Martian crust. In particular, we perform a joint inversion of Rayleigh wave ellipticity, P-to-s RFs and T_a , aiming to obtain a consolidated local crustal model.

2. Data Processing and Methods

2.1. Rayleigh Wave Ellipticity

To retrieve the characteristic ϵ at the InSight site, we performed a time-domain analysis in a similar way as has been performed on Earth (e.g., Berbellini et al., 2016; Ferreira et al., 2020; Ferreira & Woodhouse, 2007), following the steps shown in Figures 1c–1f. First, the time windows where the Rayleigh waves arrive are roughly estimated by manual inspection, following the identification by Kim, Banerdt, et al. (2022) for S1000a and S1094b and the time estimates by the Marsquake Service (MQS) for S1222a (Kawamura et al., 2022), and assuming they correspond to the fundamental mode (${}_0R_1$). These arrival time windows are shown in Figure 1c.

The raw data (InSight Mars SEIS Data Service, 2019) have been deglitched using the UCLA method (Scholz et al., 2020), restituted to ground motion (displacement) and transferred into the ZNE coordinates system. The

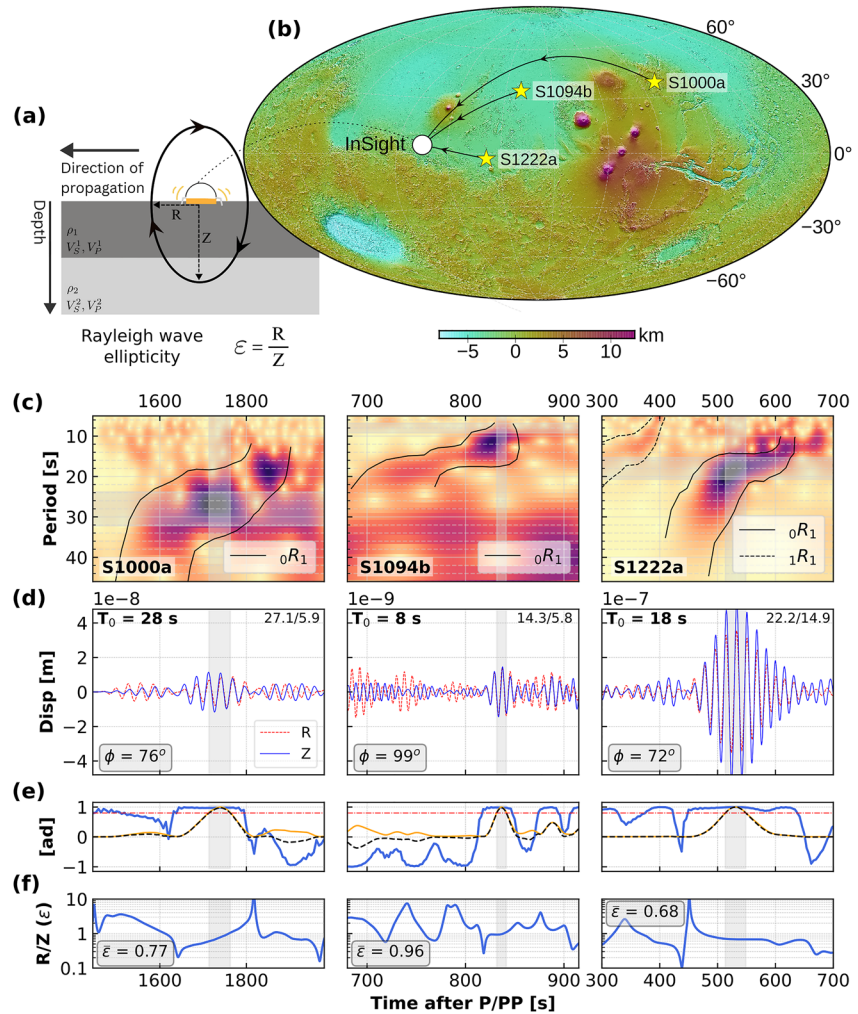


Figure 1. Rayleigh wave ellipticity from large marsquakes. (a) Schematic representation of Rayleigh wave ellipticity using the radial (R) and vertical (Z) ground motion. (b) Topographic map of Mars, from the Mars Orbiter Laser Altimeter (Smith et al., 2001), showing the epicenter of events S1000a, S1094b, S1222a and the InSight lander. Below the map, from left to right, columns correspond to events S1000a, S1094b, and S1222a, respectively. From top to bottom: (c) S-transform spectrogram of the Z component, where the fundamental mode and first overtone of the Rayleigh waves are highlighted; (d) shifted Z and R waveforms using the optimal phase shift ϕ . The Z and R components are bandpass-filtered with a 30% bandwidth around the central period T_0 , as indicated. The SNR_Z and SNR_R are given at the top right corner of each plot; (e) cross-correlation factor between shifted Z and R components (blue), normalized envelope $\eta(t)$ (yellow) and characteristic function $\chi(t)$ (dashed black). The red dot-dashed line denotes a threshold at 0.8; (f) ellipticity $\epsilon(t)$. For each event and each central period, the average ellipticity ($\bar{\epsilon}$) is computed over the time window where $\chi \geq 0.8$ (gray box).

data are then rotated into a ZRT coordinates system by using the back azimuth (BAZ) of each event. As S1000a and S1094b have been identified as impacts with source locations confirmed by orbital images (Posiolova et al., 2022), their BAZs are well constrained at around 36° and 51° , respectively. For S1222a, even though there are estimates for the location of the source (e.g., Kawamura et al., 2022), there is no ground-truth location as for S1000a and S1094b.

We applied an independent methodology to estimate the BAZ of S1222a, based on the fact that the Rayleigh waves propagate in the ZR plane. Thus, we look for the maximization of the ground-motion amplitudes on the Z and R components while minimizing the ground motion on the T component. Further details on this methodology are provided in Section S2 (Supporting Information S1). For S1222a, our estimated BAZs are in the range 114° – 137° , with a median value of 129° , which is used in this work. This BAZ is in the range obtained from the analysis of multi-orbit Rayleigh waves (Panning et al., 2022) and differs by $\sim 30^\circ$ from the BAZ derived from body waves by the MQS (Kawamura et al., 2022). After rotating into the ZRT coordinates system, the Z and R

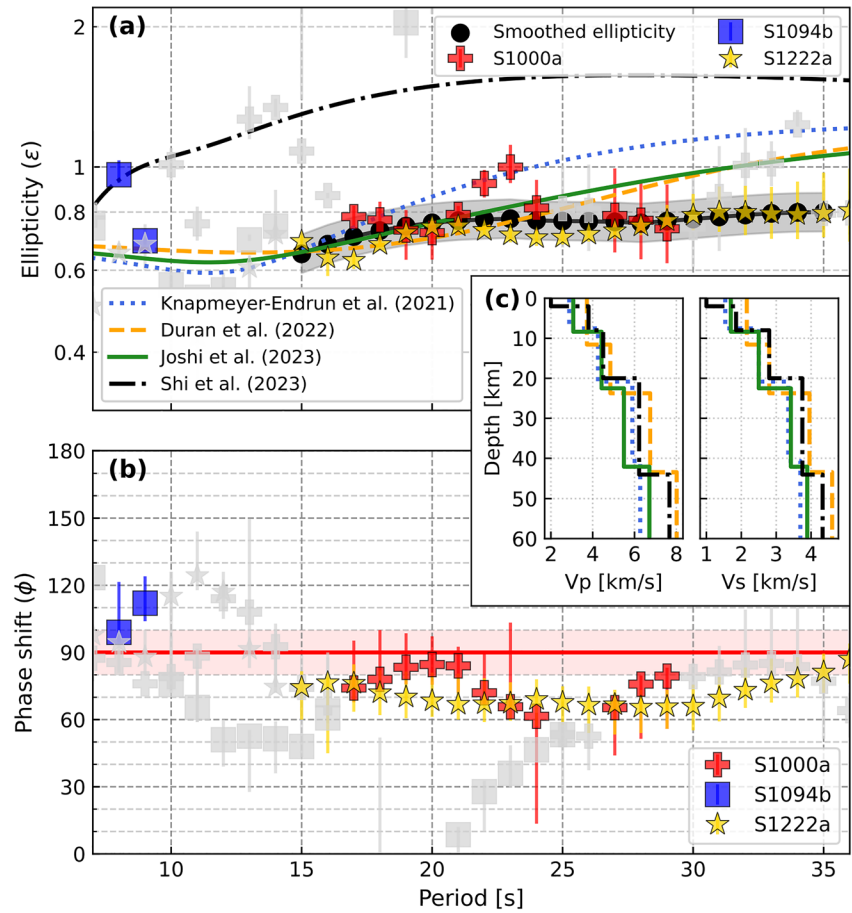


Figure 2. Rayleigh wave ellipticity and phase shift results. (a) Rayleigh wave ellipticity (ϵ) curve for events S1000a (red cross), S1094b (blue square) and S1222a (yellow star). Colored markers correspond to periods where the SNR criteria are fulfilled. Background light gray markers did not meet the minimum SNR threshold. The final ellipticity curve for the InSight site is denoted by the black circles, and a 15% uncertainty range has been imposed (gray area). Synthetic ellipticity curves are illustrated for characteristic crustal models from Knapmeyer-Endrun et al. (2021), Durán et al. (2022), Joshi et al. (2023), and Shi et al. (2023). (b) Phase shift ϕ between Z and R components of ${}_0R_1$ for the same events and with the same color code as in (a). The light red area corresponds to ϕ in the range $90 \pm 10^\circ$. (c) Vp and Vs models for the InSight crust used for synthetic calculation of ϵ in (a).

components are bandpass-filtered, with a 30% bandwidth, around different central periods T_0 (Figure 1d). In this way, every T_0 will be associated with one ellipticity value.

Subsequently, we obtained the optimal phase shift (ϕ) by maximizing the cross-correlation between the Z and R components. Examples of resulting ϕ and optimally shifted waveforms are shown in Figure 1d. Once optimally shifted, we computed the cross-correlation factor $\nu(t)$ between the shifted Z and R components (Figure 1e). The normalized envelope $\eta(t)$, also shown in Figure 1e and given by the multiplication of the Z and R envelopes, is calculated in order to find the specific time window where the energy is maximized. In order to discard low-amplitude signals with high cross-correlation (or vice versa), a characteristic function $\chi(t) = \nu(t)\eta(t)$ is calculated (Figure 1e). The final ellipticity for the central period T_0 , computed as the R/Z quotient, is the average of the ellipticities in the time window where the characteristic function χ is larger than 0.8, as shown in Figure 1f.

These processing steps are performed on the ${}_0R_1$ of events S1000a, S1094b and S1222a. In order to combine these measurements, even though radial and azimuthal anisotropy may be present, we assume that these would affect ellipticity to a lesser extent than the underlying crustal structure. To get a single characteristic ellipticity curve at the InSight landing site, only pairs of event- T_0 with actual Rayleigh wave signal are considered, that is, when the signal-to-noise ratio (SNR) is larger than a given threshold in both Z and R components. We use $\text{SNR}_Z \geq 10$ and $\text{SNR}_R \geq 5$ (given the higher noise levels on the horizontals). The final Rayleigh ellipticity curve for the InSight

site is then calculated as the smoothed median of the valid ε values, obtained by means of a Savitzky-Golay filter (Savitzky & Golay, 1964).

2.2. Joint Inversion of Ellipticity, P-To-S RFs and T_a

As the trade-off between the layer velocities and the depth of the discontinuities is a well-known feature of the ellipticity inversion, the incorporation of independent measurements such as RFs and T_a can help to further constrain the possible models (Chong et al., 2016). We thus retrieved the 1D crustal structure underneath the InSight landing site by jointly inverting the ε measurements (this work) with the mean P-to-s RF by Joshi et al. (2023), obtained by stacking radial-component low-frequency RFs for eight high-quality marsquakes mainly originating in the Cerberus Fossae region (see Joshi et al. (2023) for further details). Additionally, we included the T_a obtained by Schimmel et al. (2021), which are understood as the two-way travel times of P waves bouncing back from the first (~ 6.15 s) and second (~ 10.6 s) strong discontinuity within the crust.

For every model, the RF forward calculation is performed via a Python implementation of the code by Shibutani et al. (1996), using a fixed ray parameter $p^* = 6.9$ s/deg, suitable for events in the Cerberus Fossae region (Joshi et al., 2023). In the RF, four peaks at around 0, 2.4, 4.8, and 7.2 s are observed, which are related to the direct P phase and three converted phases P_{1s} , P_{2s} , P_{3s} , where the subscript indicates the interface where each phase is generated. The predicted ellipticity curves are obtained via the *gpell* toolbox included in the Geopsy package (Wathelet, 2005). Lastly, the T_a are computed assuming two-way vertical travel paths of the P waves.

The inversion scheme utilized is the Neighborhood Algorithm (NA), first introduced by Sambridge (1999) and widely used for multiple geophysical applications, including subsurface characterization (e.g., Carrasco et al., 2022; Ferreira et al., 2020; Hobiger et al., 2013). We applied a modified version of the NA, where the parameters space can be constrained by physical conditions and prior information (Wathelet, 2008). The parameter space is configured as 3-uniform-layers over a half-space (3LOH), where the depths of the discontinuities are constrained by Joshi et al. (2023). We inverted for shear-wave velocity V_s , P-wave velocity V_p and bottom depth z of each layer. Density was linked to V_p by using the empirical relationship by Brocher (2005), as suggested by Lin et al. (2012) for handling the trade-off with V_p/V_s , which was allowed to vary between 1.45 and 2.2. The upper mantle is modeled as a half-space with V_s between 4 and 5 km/s, following the results for the surrounding region using surface waves (Kim, Stähler, et al., 2022) and teleseismic phases (e.g., Drilleau et al., 2022; Durán et al., 2022). See Table S4 in Supporting Information S1 for further parameterization details.

The NA is based on a fully non-linear, self-adaptive Monte Carlo approach, which efficiently explores the parameters space in order to find the model \mathbf{m} that minimizes the global misfit function Ψ between the observed and theoretical data. The global misfit depends on the misfit of each data set and their weighting. In this case, we used 0.45, 0.45, and 0.1 as the weights of ε , RFs and T_a , respectively. Further details and other combinations of weights can be found in Sections S8 and S9 in Supporting Information S1.

3. Results and Discussion

3.1. Ellipticity and Phase-Shift Observations

The resulting ε and ϕ values are shown in Figures 2a and 2b, respectively. Besides the limited number of events analyzed, there is a lack of valid ellipticity measurements due to the low-amplitude energy on the radial component. The valid ε values define an ellipticity curve between 15 and 35 s and two points at 8 and 9 s (Figure 2a). For the purpose of this paper, we focus on the period range between 15 and 35 s, where the horizontal contribution of the tilt induced by Rayleigh waves can be neglected. Due to the lack of further observations, a common 15% uncertainty is utilized, which properly covers our observations.

On Earth, the ellipticity curve of one specific site is obtained from the recordings of a large number of earthquakes. In our work, even though three events were initially investigated, the ellipticity curve is mainly ruled by S1222a and, therefore, the lack of observations can be disadvantageous for further analysis and interpretation. Ellipticity data can have a large spread (e.g., Attanayake et al., 2017; Berbellini et al., 2016), which might be associated with complex Rayleigh wave propagation effects (Pedersen et al., 2015; Sexton et al., 1977) or due to local-scale heterogeneities near the receiver, as suggested by Ferreira and Woodhouse (2007) after analyzing two close stations in California. Considering the lower tectonic activity and smooth topography in the local

surrounding of InSight, as compared to the terrestrial case, we assume that the ellipticity measurements from this event can be a good representation.

Besides, the ${}_0R_1$ of S1222a has a high SNR in both Z and R components, so the final smoothed ε is expected to be a good representation of the local structure. For a better assessment, the same ellipticity analysis was performed for one station on Earth (station BQ.DREG in Germany, see Section S4 in Supporting Information S1). These measurements suggest that well-recorded events can show some variation with respect to the characteristic smoothed ellipticity curve of the site, but the broad shape of the curve remains similar. In particular, some events show different slopes and trends at specific period ranges, with respect to what is observed for the median ellipticity (Figures S3 and S4 in Supporting Information S1), but the general trend is the same. Thus, we conclude that small oscillations on the ellipticity curve should not be over-interpreted.

The resulting Z-R phase shifts, mainly ruled by S1222a, suggest ϕ values between 60° and 70° (Figure 2b), which are persistently lower than the theoretical phase shift for Rayleigh waves under isotropic and homogeneous conditions (90°). On Earth, large deviations up to $\pm 30^\circ$ have been found and have been related to small-scale heterogeneities (e.g., Ferreira & Woodhouse, 2007). From our observations on Earth, low ϕ (60 – 75°) were measured for some events at specific period ranges (see Figure S5 in Supporting Information S1). These observations suggest that anomalous ϕ might be related to the Rayleigh-wave path, or even the source, rather than the characteristics of the receiver site. Tanuma and Man (2008) also proposed that variations of ϕ with respect to the isotropic theoretical value depend on the perturbation of the initial stress conditions of the medium. Although crustal anisotropy was reported along the path of S1222a (Beghein et al., 2022; Kim, Stähler et al., 2022), its influence on the phase shift is unclear and should not be discarded. Thus, the low ϕ measured at the InSight landing site might be due to a combination of path or source effects with the initial stress conditions at this site, but not directly related to the mechanical properties of the crust at the InSight landing site. In any case, low ϕ values have previously been observed on Earth to occur in some cases. Further analysis of this phenomenon is beyond the scope of this work.

3.2. Local Crust Structure at the InSight Landing Site

In order to derive a consolidated crustal structure for the InSight landing site, the joint inversion detailed in Section 2.2 was performed. It is worth noting that the inversion of ellipticity data alone does not properly constrain the layering of the crustal structure, as different settings between one and four layers over a half-space can equally well explain the ε observations (Figure S8 in Supporting Information S1).

The initial joint inversion results suggest that these local measurements can be well explained by a three-layer model, with an overall good fitting of the three data sets (see Figure S11 in Supporting Information S1). However, the amplitude of the P-phase (first peak on the RFs), which is not normalized as it provides information on the near-surface velocities (e.g., Ammon, 1991), is clearly overestimated. As shown by synthetic forward modeling (Figure S12 in Supporting Information S1), lower amplitudes for this arrival can be achieved by having lower velocities in the first layer. Because of this, we performed a second inversion where we allowed a shallow low-velocity layer (4LOH, see Table S5 in Supporting Information S1 for details on the parameter space). These new resulting models are preferred as they explain the three independent data sets reasonably well (Figures 3a–3d), and especially the amplitude of the direct P-phase arrival is well retrieved.

Our inversion results show that a 4-layer crust structure (Figures 3e–3g), including a shallow low-velocity layer (sLVL) close to the surface, can explain the local-scale measurements well. The sLVL presents velocities between 1.6 and 1.8 km/s and extends down to 2–3 km depth. Its origin is unclear, but previous works on the shallowest structure of Mars have proposed the presence of sedimentary and heavily fractured basalt layers in the first hundreds of meters (Carrasco et al., 2022; Hobiger et al., 2021), where $V_s < 1$ km/s were derived. Furthermore, Pan et al. (2020) suggested the presence of a sedimentary layer extending from 200 to 300 m up to kilometers in depth, whereas Warner et al. (2022) showed evidence for heavily fractured basalt units in the surrounding area. Thus, we interpret this shallow discontinuity to be the bottom of this large-scale unit.

The sLVL results from combining the different data sets through the joint inversion, rather than from a specific feature of the RF. Indeed, Shi et al. (2023) showed that the ~ 1 s signal in the high-frequency RFs, related to the sLVL, is absent in the low-frequency RFs. Despite observing a similar 1 s signal in the low-frequency RF used in this work, the RF-only inversion with 3LOH shows that it is not necessarily related to an sLVL (Figure S9 in Supporting Information S1). Instead, given the mantle velocity, the ellipticity data allows a range of average

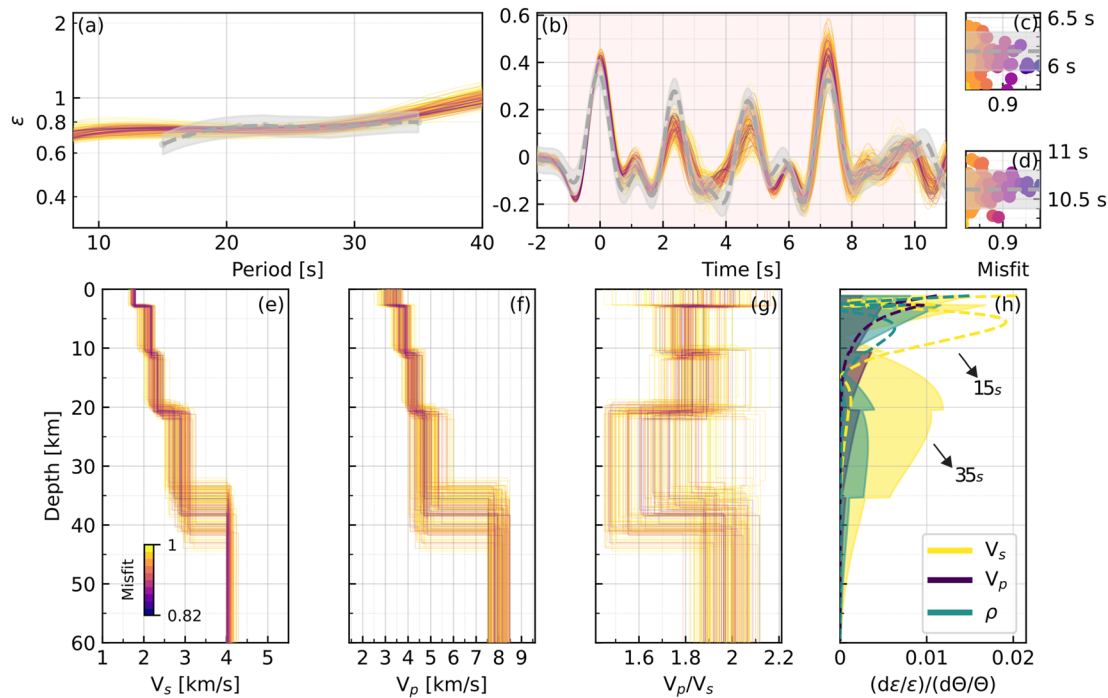


Figure 3. Joint-inversion results and resulting Martian crustal models using a 4LOH parameter space. The measurements and the synthetic modeling of 200 best-fitting crustal models are shown for (a) Rayleigh wave ellipticity, (b) P-to-s RFs from Joshi et al. (2023), and (c) first and (d) second P-wave reflection times from Schimmel et al. (2021). The light gray dashed line and area correspond to the measured data and their uncertainty, respectively, whereas the synthetic data are colored by their misfit. The corresponding crustal models are shown in terms of (e) V_s , (f) V_p , and (g) V_p/V_s , as a function of depth. (h) Depth absolute sensitivity kernels of ellipticity data for the best-fitting model, calculated at 15 s (dashed line) and 35 s (filled area) for V_s , V_p , and ρ . Light red box in (b) shows the time window where the data was fitted.

crustal V_s to fit the data, which leads to too high velocities near the surface for the RF, so a top layer with lower velocities is required.

In general, below the sLVL, our models have a similar structure and the discontinuities at ~ 10 and ~ 20 km depth are in good agreement with previously reported models for the local crust (e.g., Joshi et al., 2023; Knapmeyer-Endrun et al., 2021). The discontinuity around 37 km depth is interpreted as the crust-mantle boundary, where the sharpest velocity contrast is observed. Even though the ellipticity data has low sensitivity at this depth, it can properly constrain the shallow V_s structure (Figure 3h), which directly affects the deeper structure as they are strongly tied through the RFs. Thus, as the shallow part is well constrained, the joint inversion can provide reliable depths for the Moho.

Overall, crustal V_p and V_s are lower than 5 and 3 km/s, respectively (Figures 3e and 3f). V_p/V_s is around 1.8 in the first 20 km of the crust and, even though large variation is observed, it seems to decrease in the bottom layer of the crust (Figure 3g). In particular, V_s are lower than in other regions on Mars, such as along the path between Amazonis Planitia and the InSight site in the lowlands (Kim, Banerdt, et al., 2022), or between S1222a and the lander, along the dichotomy region (J. Li, Beghein, Lognonné, et al., 2022). Although an increase in density is derived from the inversion, the inverted data sets are poorly sensitive to this parameter, as shown for the ellipticity (Figure 3h), so further interpretation is avoided. At a local scale, our proposed V_s are also slightly lower than those previously reported for the InSight site (Joshi et al., 2023; Knapmeyer-Endrun et al., 2021). Therefore, considering that porosity plays an important role in decreasing the velocity of the seismic waves (e.g., Heap, 2019), these lower velocities might be related to an even larger porosity or stronger alteration of the whole crust at the InSight site than previously thought.

4. Conclusions

For the first time, the ellipticity of the fundamental mode of direct Rayleigh waves was measured on Mars for periods between 15 and 35 s, especially thanks to S1222a. The obtained ellipticity curve is interpreted as a good

representation of the characteristic ellipticity at the InSight landing site. Anomalously low phase shifts were measured, which seem to be unrelated to the local crust structure. In order to consolidate the local crustal model, we performed a joint inversion of local-scale observations (ellipticity, P-to-s RFs and P-wave reflection times). Our results suggest that a four-layer crustal model, with a shallow low-velocity layer of about 2–3 km thickness at the InSight landing site explains the observations well. Other discontinuities around 10, 20 and 37 km depth correlate well with previously reported models. We propose lower P- and S-wave velocities for the corresponding crustal layers, which might be related to a higher porosity or alteration of the Martian crust at the InSight landing site.

Data Availability Statement

The event information of the Martian seismic events can be found in the InSight seismic event catalog version 13 (InSight Marsquake Service, 2023). The waveform data and station metadata are available from IPGP's MSDC as well as from IRIS MDC (InSight Mars SEIS Data Service, 2019). Seismic data for station DREG (BQ network, 2016) are publicly available via EIDA (<http://eida.gfz-potsdam.de/webdc3/>). The GCMT catalog is available here <https://www.globalcmt.org/CMTsearch.html>, whereas the events analyzed for the Earth case and the codes utilized for the processing of the events can be found under <https://github.com/scarrascom/Rellipy>. Observed data used for the joint inversion, a Python implementation and preferred crustal models shown in Figure 3 can be found at <https://doi.org/10.5281/zenodo.8051337> (Carrasco, 2023). The NA was implemented via the *dinverext* plugin, which can be obtained from <http://www.geopsy.org/>.

Acknowledgments

The authors acknowledge NASA, CNES, their partner agencies and institutions (UKSA, SSO, DLR, JPL, IPGP-CNRS, ETHZ, IC and MPS-MPG), and the flight operations team at JPL, SISMOC, MSDS, IRIS-DMC and PDS for providing SEED SEIS data. Thanks to Dr. J. Li for his thoughtful comments about the manuscript. French co-authors acknowledge the French Space Agency CNES and ANR (ANR-19-CE31-0008 and ANR-18-IDEX-0001). PL, ES, ZX acknowledge IDEX Paris Cité (ANR-18-IDEX-0001). The research was carried out in part at the Jet Propulsion Laboratory, California Institute of Technology, under a contract with the National Aeronautics and Space Administration (80NM0018D0004). Open access funding enabled and organized by Projekt DEAL. This is InSight contribution ICN 299.

References

- Ammon, C. J. (1991). The isolation of receiver effects from teleseismic P waveforms. *Bulletin of the Seismological Society of America*, 81(6), 2504–2510. <https://doi.org/10.1785/bssa0810062504>
- Attanayake, J., Ferreira, A. M., Berbellini, A., & Morelli, A. (2017). Crustal structure beneath Portugal from teleseismic Rayleigh wave ellipticity. *Tectonophysics*, 712–713, 344–361. <https://doi.org/10.1016/j.tecto.2017.06.001>
- Banerdt, W., Smrekar, S., Banfield, D., Giardini, D., Golombek, M., Johnson, C. L., et al. (2020). Initial results from the InSight mission on Mars. *Nature Geoscience*, 13(3), 183–189. <https://doi.org/10.1038/s41561-020-0544-y>
- Beghein, C., Li, J., Weidner, E., Maguire, R., Wokey, J., Lekić, V., et al. (2022). Crustal Anisotropy in the Martian lowlands from surface waves. *Geophysical Research Letters*, 49(24), e2022GL101508. <https://doi.org/10.1029/2022gl101508>
- Berbellini, A., Morelli, A., & Ferreira, A. M. (2016). Ellipticity of Rayleigh waves in basin and hard-rock sites in Northern Italy. *Geophysical Journal International*, 206(1), 395–407. <https://doi.org/10.1093/gji/ggw159>
- Berbellini, A., Morelli, A., & Ferreira, A. M. G. (2017). Crustal structure of northern Italy from the ellipticity of Rayleigh waves. *Physics of the Earth and Planetary Interiors*, 265, 1–14. <https://doi.org/10.1016/j.pepi.2016.12.005>
- BQ network. (2016). Bensberg earthquake network. International federation of digital seismograph networks. <https://doi.org/10.7914/SN/BQ>
- Brocher, T. M. (2005). Empirical relations between elastic wavespeeds and density in the Earth's crust. *Bulletin of the Seismological Society of America*, 95(6), 2081–2092. <https://doi.org/10.1785/0120050077>
- Carrasco, S. (2023). Martian crustal models at the InSight landing site from joint inversion of ellipticity, P-to-s RFs and autocorrelations times. *Zenodo*. <https://doi.org/10.5281/zenodo.8051337>
- Carrasco, S., Knapmeyer-Endrun, B., Margerin, L., Schmelzbach, C., Onodera, K., Pan, L., et al. (2022). Empirical H/V spectral ratios at the InSight landing site and implications for the martian subsurface structure. *Geophysical Journal International*, 232(2), 1293–1310. <https://doi.org/10.1093/gji/ggac391>
- Chong, J., Ni, S., Chu, R., & Somerville, P. (2016). Joint inversion of body-wave receiver function and Rayleigh-wave ellipticity. *Bulletin of the Seismological Society of America*, 106(2), 537–551. <https://doi.org/10.1785/0120150075>
- Drilleau, M., Samuel, H., Garcia, R. F., Rivoldini, A., Perrin, C., Michaut, C., et al. (2022). Marsquake locations and 1-D seismic models for Mars from InSight data. *Journal of Geophysical Research: Planets*, 127(9), e2021JE007067. <https://doi.org/10.1029/2021je007067>
- Durán, C., Khan, A., Ceylan, S., Zenhäusern, G., Stähler, S., Clinton, J., & Giardini, D. (2022). Seismology on Mars: An analysis of direct, reflected, and converted seismic body waves with implications for interior structure. *Physics of the Earth and Planetary Interiors*, 325, 106851. <https://doi.org/10.1016/j.pepi.2022.106851>
- Ferreira, A. M., Marignier, A., Attanayake, J., Frietsch, M., & Berbellini, A. (2020). Crustal structure of the Azores Archipelago from Rayleigh wave ellipticity data. *Geophysical Journal International*, 221(2), 1232–1247. <https://doi.org/10.1093/gji/ggaa076>
- Ferreira, A. M., & Woodhouse, J. H. (2007). Observations of long period Rayleigh wave ellipticity. *Geophysical Journal International*, 169(1), 161–169. <https://doi.org/10.1111/j.1365-246x.2006.03276.x>
- Heap, M. J. (2019). P- and S-wave velocity of dry, water-saturated, and frozen basalt: Implications for the interpretation of Martian seismic data. *Icarus*, 330, 11–15. <https://doi.org/10.1016/j.icarus.2019.04.020>
- Hobiger, M., Cornou, C., Wathelet, M., Giulio, G. D., Knapmeyer-Endrun, B., Renalier, F., et al. (2013). Ground structure imaging by inversions of Rayleigh wave ellipticity: Sensitivity analysis and application to European strong-motion sites. *Geophysical Journal International*, 192(1), 207–229. <https://doi.org/10.1093/gji/ggs005>
- Hobiger, M., Hallo, M., Schmelzbach, C., Stähler, S., Fäh, D., Giardini, D., et al. (2021). The shallow structure of Mars at the InSight landing site from inversion of ambient vibrations. *Nature Communications*, 12(1), 6756. <https://doi.org/10.1038/s41467-021-26957-7>
- InSight Marsquake Service. (2023). Mars seismic catalogue, InSight mission; V13 2023-01-01 (version 13.0) [dataset]. ETHZ, IPGP, JPL, ICL, Univ. Bristol. <https://doi.org/10.12686/a19>
- InSight Mars SEIS Data Service. (2019). SEIS raw data, InSight Mission. IPGP, JPL, CNES, ETHZ, ICL, MPS, ISAE-Supaero, LPG, MFSC. https://doi.org/10.18715/SEIS.INSIGHT.XB_2016

- Joshi, R., Knapmeyer-Endrun, B., Mosegaard, K., Wicczorek, M. A., Igel, H., Christensen, U., & Lognonné, P. H. (2023). Joint Inversion of receiver functions and apparent incidence angles to determine the crustal structure of Mars. *Geophysical Research Letters*, 50(3), e2022GL100469. <https://doi.org/10.1029/2022GL100469>
- Kawamura, T., Clinton, J. F., Zenhäusern, G., Ceylan, S., Horleston, A. C., Dahmen, N. L., et al. (2022). S1222a - The largest Marsquake detected by InSight. *Geophysical Research Letters*, 50(5), e2022GL101543. <https://doi.org/10.1029/2022GL101543>
- Kim, D., Banerdt, W., Ceylan, S., Giardini, D., Lekić, V., Lognonné, P., et al. (2022). Surface waves and crustal structure on Mars. *Science*, 378(6618), 417–421. <https://doi.org/10.1126/science.abq7157>
- Kim, D., Lekić, V., Irving, J. C., Schmerr, N., Knapmeyer-Endrun, B., Joshi, R., et al. (2021). Improving constraints on planetary interiors with PPS receiver functions. *Journal of Geophysical Research: Planets*, 126(11), e2021JE006983. <https://doi.org/10.1029/2021je006983>
- Kim, D., Stähler, S. C., Ceylan, S., Lekic, V., Maguire, R., Zenhäusern, G., et al. (2022). Structure along the Martian dichotomy constrained by Rayleigh and love waves and their overtones. *Geophysical Research Letters*, 50(8), e2022GL101666. <https://doi.org/10.1029/2022GL101666>
- Knapmeyer-Endrun, B., Panning, M., Bissig, F., Joshi, R., Khan, A., Kim, D., et al. (2021). Thickness and structure of the martian crust from InSight seismic data. *Science*, 373(6553), 438–443. <https://doi.org/10.1126/science.abc8966>
- Li, G., Chen, H., Niu, F., Guo, Z., Yang, Y., & Xie, J. (2016). Measurement of Rayleigh wave ellipticity and its application to the joint inversion of high-resolution S wave velocity structure beneath northeast China. *Journal of Geophysical Research: Solid Earth*, 121(2), 864–880. <https://doi.org/10.1002/2015jb012459>
- Li, J., Beghein, C., Davis, P., Wicczorek, M. A., McLennan, S. M., Kim, D., et al. (2022). Crustal structure constraints from the detection of the SsPp phase on Mars. *Earth and Space Science*, e2022EA002416. <https://doi.org/10.1029/2022EA002416>
- Li, J., Beghein, C., Lognonné, P., McLennan, S. M., Wicczorek, M., Panning, M., et al. (2022). Different Martian crustal seismic velocities across the dichotomy boundary from multi-orbiting surface waves. *Geophysical Research Letters*, e2022GL101243. <https://doi.org/10.1029/2022GL101243>
- Li, J., Beghein, C., McLennan, S. M., Horleston, A. C., Charalambous, C., Huang, Q., et al. (2022). Constraints on the martian crust away from the InSight landing site. *Nature Communications*, 13(1), 7950. <https://doi.org/10.1038/s41467-022-35662-y>
- Li, J., Beghein, C., Wookey, J., Davis, P., Lognonné, P., Schimmel, M., et al. (2022). Evidence for crustal seismic anisotropy at the InSight lander site. *Earth and Planetary Science Letters*, 593, 117654. <https://doi.org/10.1016/j.epsl.2022.117654>
- Lin, F.-C., Schmandt, B., & Tsai, V. C. (2012). Joint inversion of Rayleigh wave phase velocity and ellipticity using USArray: Constraining velocity and density structure in the upper crust. *Geophysical Research Letters*, 39(12). <https://doi.org/10.1029/2012gl016529>
- Lognonné, P., Banerdt, W., Pike, W., Giardini, D., Zweifel, P., Garcia, R. F., et al. (2020). Constraints on the shallow elastic and anelastic structure of Mars from InSight seismic data. *Nature Geoscience*, 13(3), 213–220. <https://doi.org/10.1038/s41561-020-0536-y>
- Lognonné, P., Banerdt, W. B., Giardini, D., Pike, W. T., Christensen, U., Laudet, P., et al. (2019). SEIS: InSight's seismic experiment for internal structure of Mars. *Space Science Reviews*, 215(1), 1–170. <https://doi.org/10.1007/s11214-018-0574-6>
- Pan, L., Quantin-Nataf, C., Tauzin, B., Michaut, C., Golombek, M., Lognonné, P., et al. (2020). Crust stratigraphy and heterogeneities of the first kilometers at the dichotomy boundary in western Elysium Planitia and implications for InSight lander. *Icarus*, 228, 113511. <https://doi.org/10.1016/j.icarus.2019.113511>
- Panning, M. P., Banerdt, W. B., Beghein, C., Carrasco, S., Ceylan, S., Clinton, J. F., et al. (2022). Locating the largest event observed on Mars with multi-orbit surface waves. *Geophysical Research Letters*, 50(1), e2022GL101270. <https://doi.org/10.1029/2022GL101270>
- Panning, M. P., Lognonné, P., Bruce Banerdt, W., Garcia, R., Golombek, M., Kedar, S., et al. (2017). Planned products of the Mars structure service for the InSight mission to Mars. *Space Science Reviews*, 211(1), 611–650. <https://doi.org/10.1007/s11214-016-0317-5>
- Pedersen, H., Boué, P., Poli, P., & Colombi, A. (2015). Arrival angle anomalies of Rayleigh waves observed at a broadband array: A systematic study based on earthquake data, full waveform simulations and noise correlations. *Geophysical Supplements to the Monthly Notices of the Royal Astronomical Society*, 203(3), 1626–1641. <https://doi.org/10.1093/gji/ggv382>
- Posiolova, L. V., Lognonné, P., Banerdt, W. B., Clinton, J., Collins, G. S., Kawamura, T., et al. (2022). Largest recent impact craters on Mars: Orbital imaging and surface seismic co-investigation. *Science*, 378(6618), 412–417. <https://doi.org/10.1126/science.abq7704>
- Sambridge, M. (1999). Geophysical inversion with a neighbourhood algorithm—I. Searching a parameter space. *Geophysical Journal International*, 138(2), 479–494. <https://doi.org/10.1046/j.1365-246x.1999.00876.x>
- Savitzky, A., & Golay, M. J. (1964). Smoothing and differentiation of data by simplified least squares procedures. *Analytical Chemistry*, 36(8), 1627–1639. <https://doi.org/10.1021/ac60214a047>
- Schimmel, M., Stutzmann, E., Lognonné, P., Compaire, N., Davis, P., Drilleau, M., et al. (2021). Seismic noise autocorrelations on Mars. *Earth and Space Science*, 8(6), e2021EA001755. <https://doi.org/10.1029/2021EA001755>
- Scholz, J.-R., Widmer-Schmidrig, R., Davis, P., Lognonné, P., Pinot, B., Garcia, R., et al. (2020). Detection, analysis, and removal of glitches from InSight's seismic data from Mars. *Earth and Space Science*, 7(11). <https://doi.org/10.1029/2020EA001317>
- Sexton, J. L., Rudman, A., & Mead, J. (1977). Ellipticity of Rayleigh waves recorded in the Midwest. *Bulletin of the Seismological Society of America*, 67(2), 369–382. <https://doi.org/10.1785/bssa0670020369>
- Shi, J., Plasman, M., Knapmeyer-Endrun, B., Xu, Z., Kawamura, T., Lognonné, P., et al. (2023). High-frequency receiver functions with event S1222a reveal a discontinuity in the Martian shallow crust. *Geophysical Research Letters*, 50(5), e2022GL101627. <https://doi.org/10.1029/2022GL101627>
- Shibutani, T., Sambridge, M., & Kennett, B. (1996). Genetic algorithm inversion for receiver functions with application to crust and uppermost mantle structure beneath eastern Australia. *Geophysical Research Letters*, 23(14), 1829–1832. <https://doi.org/10.1029/96gl01671>
- Smith, D. E., Zuber, M. T., Frey, H. V., Garvin, J. B., Head, J. W., Muhleman, D. O., et al. (2001). Mars orbiter laser altimeter: Experiment summary after the first year of global mapping of Mars. *Journal of Geophysical Research*, 106(E10), 23689–23722. <https://doi.org/10.1029/2000je001364>
- Tanimoto, T., & Rivera, L. (2008). The ZH ratio method for long-period seismic data: Sensitivity kernels and observational techniques. *Geophysical Journal International*, 172(1), 187–198. <https://doi.org/10.1111/j.1365-246x.2007.03609.x>
- Tanuma, K., & Man, C.-S. (2008). Perturbation formulas for polarization ratio and phase shift of Rayleigh waves in prestressed anisotropic media. *Journal of Elasticity*, 92(1), 1–33. <https://doi.org/10.1007/s10659-007-9147-8>
- Warner, N., Golombek, M., Ansan, V., Marteau, E., Williams, N., Grant, J., et al. (2022). In situ and orbital stratigraphic characterization of the InSight landing site—A type example of a regolith-covered lava plain on Mars. *Journal of Geophysical Research: Planets*, 127(4). <https://doi.org/10.1029/2022JE007232>
- Wathelet, M. (2005). *Array recordings of ambient vibrations: Surface-wave inversion*. PhD Diss (p. 161). Liège University.
- Wathelet, M. (2008). An improved neighborhood algorithm: Parameter conditions and dynamic scaling. *Geophysical Research Letters*, 35(9), L09301. <https://doi.org/10.1029/2008GL032556>

- Wieczorek, M. A., Broquet, A., McLennan, S. M., Rivoldini, A., Golombek, M., Antonangeli, D., et al. (2022). InSight constraints on the global character of the martian crust. *Journal of Geophysical Research: Planets*, 127(5), e2022JE007298. <https://doi.org/10.1029/2022JE007298>
- Xu, Z., Broquet, A., Fuji, N., Kawamura, T., Lognonné, P., Montagner, J.-P., et al. (2023). Investigation of martian regional crustal structure near the dichotomy using S1222a surface-wave group velocities. *Geophysical Research Letters*, 50(8), e2023GL103136. <https://doi.org/10.1029/2023gl103136>
- Yano, T., Tanimoto, T., & Rivera, L. (2009). The ZH ratio method for long-period seismic data: Inversion for S-wave velocity structure. *Geophysical Journal International*, 179(1), 413–424. <https://doi.org/10.1111/j.1365-246x.2009.04293.x>